Journal of Power Sources 195 (2010) 2709–2717

Contents lists available at ScienceDirect

Journal of Power Sources

journal homepage: www.elsevier.com/locate/jpowsour

Gradation of mechanical properties in gas diffusion electrode. Part 1: Influence of nano-scale heterogeneity in catalyst layer on interfacial strength between catalyst layer and membrane

K.K. Poornesh [a], C.D. Cho [a,*], G.B. Lee [b], Y.S. Tak [b]

[a] iASME Laboratory, Department of Mechanical Engineering, Inha University, 253 Yonghyun-Dong, Nam-Ku, Inchon, 402-751, South Korea
[b] Materials and Electro-Chemistry Laboratory, Department of Chemical Engineering, Inha University, Incheon, South Korea

ARTICLE INFO

Article history:
Received 10 October 2009
Received in revised form
17 November 2009
Accepted 25 November 2009
Available online 1 December 2009

Keywords:
Catalyst layer
Contact stiffness
Gradation
Modulus
Plastic strain
Stress redistribution

ABSTRACT

Stress and plastic deformation analyses of catalyst layer have been conducted after experimentally investigating its mechanical properties at nano-scale. Interestingly, catalyst layer is found to have varying mechanical properties as a function of depth and therefore it is classified under graded material. Effect of gradation in catalyst layer on interfacial strength between membrane and catalyst layer is explained with the aid of numerical simulations. Stress redistribution near interface line is observed in graded model, while stresses are found to have concentrated at critical locations throughout the discrete model. However, it is outlined from this study that the gradation in catalyst layer leads to greater amount of plastic energy dissipation—an indication of enhanced ductility. An experimental coupled numerical approach is presented to characterize the effect of transitional variations of mechanical properties in catalyst layer on the interfacial line and membrane.

1. Introduction

Graded materials are classes of materials where structural and mechanical properties vary as a function of depth. Some natural examples of these include bamboo, bone and some biological structures [1–3]. Learning from the nature, biological structures self-evolve in developing material layers to protect themselves from the external forces. Imitating the structural integrity principles involved in these structures (focused on material gradation), innovative materials can be made available for engineering applications. In structural applications, graded materials find their major role in sustaining greater amount of stresses and thereby functioning as a damage resistant [4]. This concept can be advantageous in the interfacial contact regions where force transmission takes place, particularly between two dissimilar materials such as gas diffusion layer (GDL) and nafion membrane. However, the choice of gradation in any engineered material must be reasonable. In a PEM fuel cell, catalyst layer (here after it is denoted as CL) work as an interfacial layer between GDL and membrane. It is later found in this study that CL belongs to a class of graded materials. The choice of CL as a graded material was totally unintentional (spray coated on GDL) which raises an important question – whether this gradation is desirable under PEM fuel cell loading/operating conditions or not? External loading and material property varying directions are the two basic parameters to be considered in utilizing the graded material for a desired application (employing a continuously graded material near the interface would suppress the evolution of crack or permanent plastic deformation [5]). Vital information in terms of modulus or stiffness variation from a graded material surface to the bottom level can be helpful in quantifying the stress concentration and related failure mechanisms. If CL acts as a 'smooth transition zone' (caused due to gradation in its composition) between GDL and membrane, it will reduce the crack driving force throughout the interface by maintaining a good interfacial bond. Gradation can be defined over a single layer and/or when its definition is applied to the whole system, it will be referred as a 'graded system'. MEA (membrane electrode assembly) is one perfect example for a 'graded system', where an individual-layer has a different modulus and yield/failure limits and its values are expected to decrease in an exponential or stepwise (absence of smooth gradation) manner. However, it is too early to comment further on its effect on the structural integrity of the fuel cell system without being studied about the interfacial CL. Hence, in our current study we deal with a thorough investigation on mechanical property variation in CL from its surface to the bottom.

* Corresponding author. Tel.: +82 32 860 7321; fax: +82 32 868 1716.
E-mail address: cdcho@inha.ac.kr (C.D. Cho).

0378-7753/$ – see front matter © 2009 Elsevier B.V. All rights reserved.
doi:10.1016/j.jpowsour.2009.11.101

On the other hand, from a macroscopic perspective, degradation of fuel cell parts largely depends upon the fabrication and operating conditions as well as on the individual-layer material properties. Structural durability of MEA is one of the areas where morphological defects do exist [6,7] and may lead to severe mechanical failure modes. It is believed that fuel cell working conditions such as varying temperature, humidity and external compressive load are the primary factors for 'mechanical degradation' in the interfacial region between membrane and CL. Studying the structural response of MEA through numerical simulation under the cell operating conditions will give much knowledge about actual underlying principles of failure. Numerical simulation of cracks in bulk CL and delaminations between the cell layers (membrane and CL) becomes more challenging given the nature of complexity in assigning the material properties for CL. Lack of understandings about mechanical characterization of CL certainly hinders the simulation capabilities to predict the failure. Recent developments related to structural analyses can be found elsewhere [8–11]. All of the structural simulations done to date have assumed CL and gas diffusion layer as a one single layer referred as gas diffusion electrode (GDE) due to the unknown mechanical properties of CL.

Nafion and Pt/C black are the major constituents of CL. In general, distribution of pores and networks depends on these constituents' distribution and fabrication process. Studies [12,13] show that performance of cathode electrode is directly influenced by the distribution of nafion content (multilayered catalyst coating) and better results are expected when nafion content is higher toward membrane than toward GDL. In other words, CL is said to have 'graded', when there is a non-uniform distribution of nafion content. However, like in our case, when a single CL is coated over GDL, nafion distribution would be uniform. Hence, on mechanical perspective, it is presumed in our study that nafion is a binder material and Pt/C particles are spatially distributed. From now on, the CL would be classified as a 'graded' or 'uniform' based on the Pt/C particle distribution and not by the binder material.

For our experimental investigation, instrumented indentation, also referred as 'nanoindentation' is opted for mechanical characterization of CL. Nanoindentation is commonly used for measuring nano- or microscale mechanical properties of thin films. However its application is not only limited to films. This technique has become ubiquitous in characterizing the mechanical properties of materials whose properties are size or small volume dependent. Recently, nanoindentation has been applied to characterize the mechanical properties of nanowires [14,15], CNTs [16], amorphous carbon films [17], nanobelts [18], biological tissues [19,20], and nanocomposites [21]. The obtained values of load and displacement as a function of depth or time are used to calculate the hardness and elastic modulus. It is also possible to establish a relation between contact stiffness and displacement and from this, material under investigation can be classified as a graded or uniform one. Sensing its capability to characterize the individual constituents within the heterogeneous sample, it can well be adopted in obtaining the mechanical parameters of CL.

Experimental data obtained from indentation is used in combination with the FEA (finite element analysis) to evaluate the yield strength and resulting stresses in catalyst layer. Indentation behavior of combined CL and membrane (in our present investigation it will be referred as a dual-layer system) is also studied numerically. Discrete and graded models with two different layers (membrane and CL) having the same material model (elastic–plastic) are opted for our present study. It will be interesting to see on how these mechanical gradations affect the indentation behavior of discrete CL as well as on dual-layer models.

2. Experimental

In the following, procedure adopted in preparing CL is explained. The carbon slurry was prepared by mixing carbon black (Vulcan XC72, Cabot) vigorously with the distilled water. Then this mixture was heated to 90 °C. The pH of the slurry was adjusted to the basic using NaOH. The chloroplatinic acid (H_2PtCl_6, Aldrich) solution, prepared by dissolving into the distilled water, was added to the carbon slurry and the pH of the slurry was again adjusted to the basic. Reducing agent was then introduced into the slurry for in situ liquid phase reduction. The Pt/C mixture was filtered, washed, and then dried at 90 °C. From now on 20 wt% Pt/C catalyst referred as Pt/C-1. Catalyst ink was prepared by dispersing Pt/C catalyst in a mixed solution of ethanol and nafion. Prepared catalyst ink was coated on GDL (Carbon paper, Toray) using spray technique. Pt loading was 0.15 mg cm^{-2}. Same procedure is followed in preparing the 20 wt% Johnson–Matthey based catalyst layer (here after it is referred as J–M).

For mechanical characterization, samples (Pt/C-1 and J–M) of 0.5 cm^2 were carefully cut and subjected to indentation testing. Nano indenter G200 (MTS corp.) with Berkovich diamond indenter tip was used for our experimental investigations. Samples were mounted on sample disk, which was initially heated using heating element to appropriate temperature in order to bond the sample and disk using small amount of crystalbond.

3. Analytical

In general, contact on graded material can be typified as elastic or plastic. Corresponding numerical modeling also follows the same material models. In the elastic graded material, either modulus increases or decreases from a surface level to the bottom, linearly or nonlinearly. In contrast to homogeneous material, graded model must involve these gradations as a function of material thickness. Quantifying a material for its contact stiffness can be very informative in predicting its strength as a function of depth. It is now understandable that modulus and hardness are dependable on material stiffness throughout the material thickness. On the other hand, indentation modeling of graded material under plastic material model requires an estimation of the yield strength. Further, the yield strength of a graded material varies as a function of depth and thus numerical modeling becomes even more challenging than the elastic case.

Fig. 1(a) shows the schematic diagram of indentation on graded material (non-uniform particle distribution). Generalizing the results obtained in the literature [1,21] one can predict the contact stiffness response of graded material to be nonlinear for an increasing indentation depth. This gives information related to the particle distributions in a material. Initial increase in contact stiffness for a small indentation depth is attributed to the densely packed particles on a surface level. Fig. 1(a) is a typical case where slope of the stiffness curve decreases, indicating a decreasing modulus of the material. If the slope increases upon indentation depth, material is possessed to have an exactly opposite behavior (increasing gradation). Fig. 1(b) shows a schematic representation of indentation on uniform material. Corresponding response of contact stiffness as a function of indentation depth is linear. Fig. 1(c) depicts a typical indentation curve for loading and unloading response of a material as a function of indenter displacement. This curve is used to obtain important mechanical parameters such as modulus and hardness. Contact stiffness, S, can be obtained from the slope of the initial part (straight line) of the unloading curve that can then be used to calculate the reduced modulus using a following

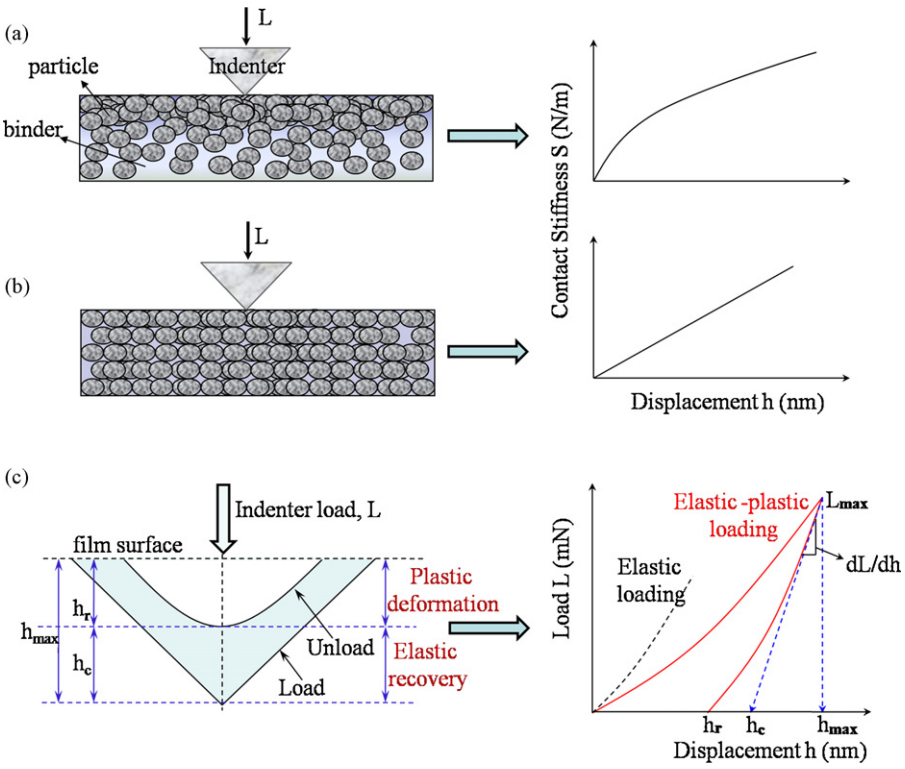

Fig. 1. Nanoindentation response (a) schematic representation of indentation on graded material. Corresponding contact stiffness vs indentation depth is expected to be nonlinear as shown on right side of the figure. (b) Indentation on uniforma material and its response to contact stiffness is likely to be linear (right side). (c) Typical indentation curve, showing the loading and unloading cycle. Residual impression is expected upon indentation in elasto-plastic material.

Eq. (1) [22]:

$$S = \left(\frac{2}{\sqrt{\pi}}\right) E_r \sqrt{A_P} \tag{1}$$

where E_r is reduced modulus and A_p is the projected area on the specimen by the indenter. Eq. (1) holds well when unloading curve is almost linear. However most of the unloading curves are not linear, hence, curve is fitted according to power law defined over indentation load L:

$$L = C(h - h_r)^m \tag{2}$$

where C and m are fitting parameters and h is the indentation depth. Differentiating Eq. (2) with respect to the indentation depth following relation can be obtained for S:

$$\left(\frac{dL}{dh}\right)_{h=h_{\max}} = mC(h_{\max} - h_r)^{m-1} = S \tag{3}$$

Now, reduced modulus E_r can be calculated using Eq. (4):

$$\frac{1}{E_r} = \frac{1-\upsilon_s^2}{E_s} + \frac{1-\upsilon_i^2}{E_i} \tag{4}$$

Diamond indenter modulus, E_i, and Poisson's ratio, υ_i, are taken as 1140 GPa and 0.07, respectively. E_s and υ_s (assumed 0.18) are the modulus and Poisson's ratio of the material. Further, for Berkovich indenter, relationship between projected contact area and contact depth is given by Eq. (5) [17]:

$$A(h_c) = 24.5(h_c)^2 \tag{5}$$

and

$$h_c = h_{\max} - \varepsilon(h_{\max} - h_r) \tag{6}$$

where h_c is the contact depth and $h_{\max}$ is the maximum displacement at a maximum load $L_{\max}$. h_r is the depth of the residual impression. For Berkovich indenter, geometry correction factor ε is 0.75 [22]. Fig. 1(c) can be referred to understand the parameters involved in Eq. (6). Mean contact pressure, p_m, is a measure of indentation hardness, H, and is defined as the amount of indentation load, $L_{\max}$, over projected area of the contact surface, and is given by Eq. (7).

$$p_m = \frac{L_{\max}}{A_P} = \frac{dW}{A_P dh} = \frac{dW}{dV_I} \tag{7}$$

where dW is the change in external indentation work and dV_I is the change in indented volume (product of projected area and indentation depth). The internal energy of elastic–plastic material subjected to indentation can be separated into two parts, elastic energy, E_e, and plastic energy, E_p, and is given by Eq. (8).

$$E_I = \underbrace{\int_{V_I} (\sigma_{ij} d\varepsilon_{ij})_e dV_I}_{\text{elastic energy}(E_e)} + \underbrace{\int_{V_I} (\sigma_{ij} d\varepsilon_{ij})_p dV_I}_{\text{plastic energy dissipation}(E_p)} \tag{8}$$

where σ and ε represents the stress and strain, respectively. Again, any change in external work leads to change in internal energy, hence, dW in Eq. (7) corresponds to dE_I. From Eqs. (7) and (8) we can have:

$$dW = dE_e + dE_p = p_m dV_I \tag{9}$$

Finally mean contact pressure can be rewritten as follows:

$$p_m = \partial E_{e,V_I} + \partial E_{p,V_I} = p_e + p_p \tag{10}$$

This is similar to an expression obtained in [5], where p_e and p_p are the elastic and plastic contributions, respectively.

4. Finite element analyses

Average indentation load–displacement data obtained from nanoindentation is fitted to elastic–perfectly plastic CL (no grada-

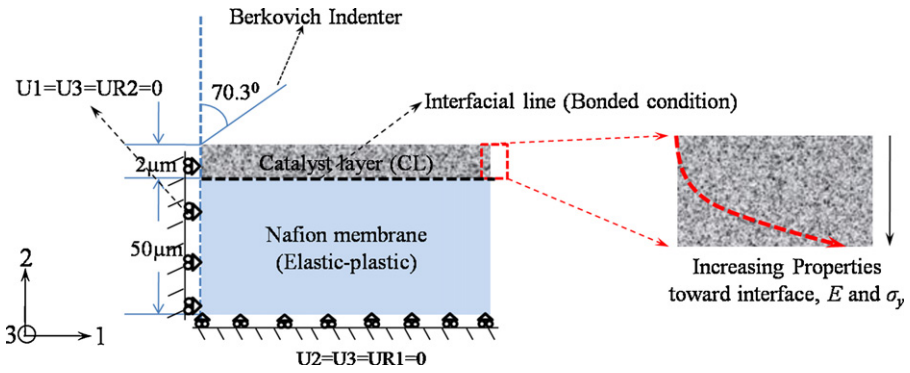

Fig. 2. Axisymmetric simulation model for graded dual-layer model comprising membrane and graded CL. Constrained displacements in direction-1 and direction-2 are applied at the bottom boundary line and left side boundary line, respectively. Enlarged view of CL shows the increasing gradation in material properties from top to bottom surface.

tion or discrete) model developed through ABAQUS FE commercial package [23] to determine the yield strength. Indentation on CL as well as dual-layer (membrane and CL) is studied for the distribution of stresses and the level of plastic deformation. As of now, GDL is not considered, since our major focus is on CL and its effect on load transferring characteristics to the membrane under discrete as well as graded conditions. In graded model, modulus is varied according to the experimentally obtained values as a function of depth. The yield strength values are obtained by scaling down the experimentally obtained hardness data and are taken as a function of depth under zero work hardening condition. To enable this to function, a user defined material subroutine (UMAT) is written for the graded CL. Further, results are compared with a discrete model and it is our interest to know how these changes will affect the stress distribution in various material directions. (It is noted that, although CL is a highly porous layer, it can well be taken as a thin 2D solid section for the numerical analyses, since the mechanical properties obtained from the indentation experiment represents the effective response of CL and hence are influenced by its constituents (see Section 5.2).)

Properties of nafion membrane are already established [10,11] and are modeled as an elastic–plastic material under ambient conditions (25 °C and 30% RH). Fig. 2 shows the schematic of the FE model and boundary conditions. Four node bilinear axisymmetric CAX4R quadrilateral elements, available in ABAQUS element library are used for all cell layers. Berkovich indenter is modeled as an axisymmetric 2D-half cone with an angle of 70.3° to the vertical axis. Tip radius was taken to be around 100 nm and was modeled as a rigid. Contacting bodies are given frictionless contact. Since the problem involves a large deformation near the contact between catalyst surface and the indenter, mesh convergence is given high importance and is studied for obtaining accurate results.

5. Results and discussions

5.1. Physical characterization

Pt/C-1 and J–M catalysts are initially studied for their structural characteristics. This is done to quantify that the indentation characteristics obtained here are true for only Pt/C based catalyst. Ex situ TEM measurements of Pt/C-1 as well as J–M catalysts are done to characterize the particle size, particle shape and particle distribution of electro-catalysts. Fig. 3(a) shows the TEM micrograph of commercial (J–M) catalyst with small Pt particles distributed on grey carbon support (about 30 nm). Aggregation of particles is seen with an average particle size of 3.4 nm. Fig. 3(b) shows the TEM micrograph of Pt/C-1 with an average particle size of 2.8 nm and particles are well dispersed on carbon support. Although TEM

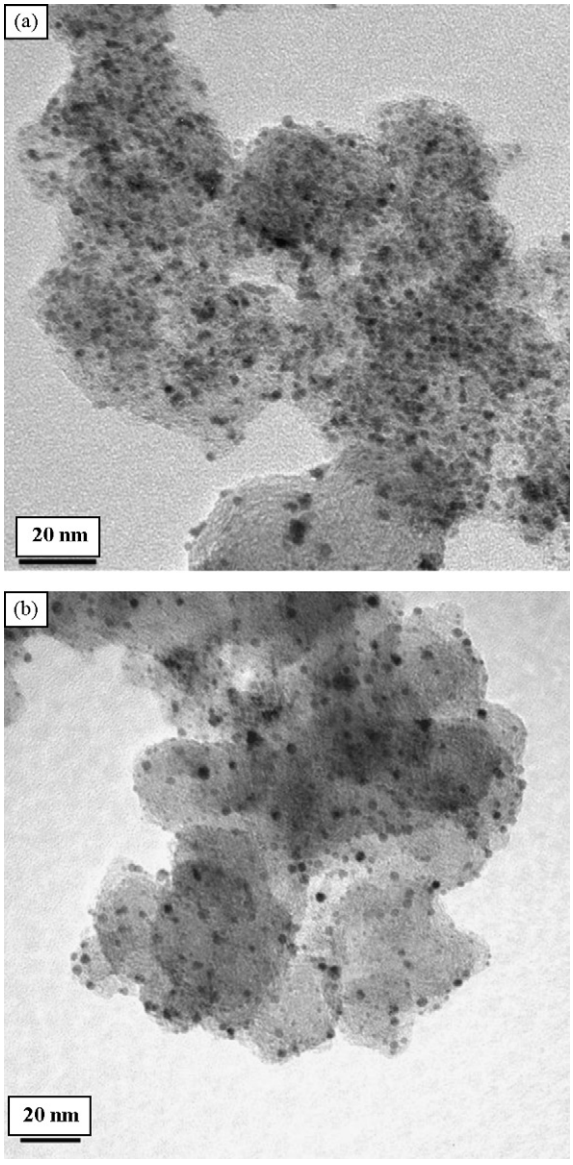

Fig. 3. TEM micrographs of (a) J–M. (b) Pt/C-1.

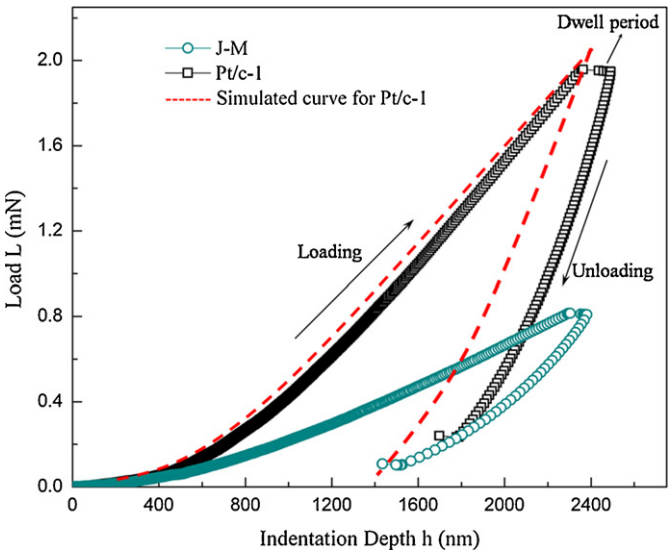

Fig. 4. Nanoindentation results for J–M and Pt/C-1 catalysts in terms of load and indentation depth. Load required for J–M catalyst to indent 2000 nm is observed to be far less than in case of Pt/C-1 catalyst. Modulus and hardness values are obtained directly from the experiment. Red-dotted lines shows the curve fit for Pt/C-1 catalyst to obtain yield strength. (For interpretation of the references to color in the figure caption, the reader is referred to the web version of the article.)

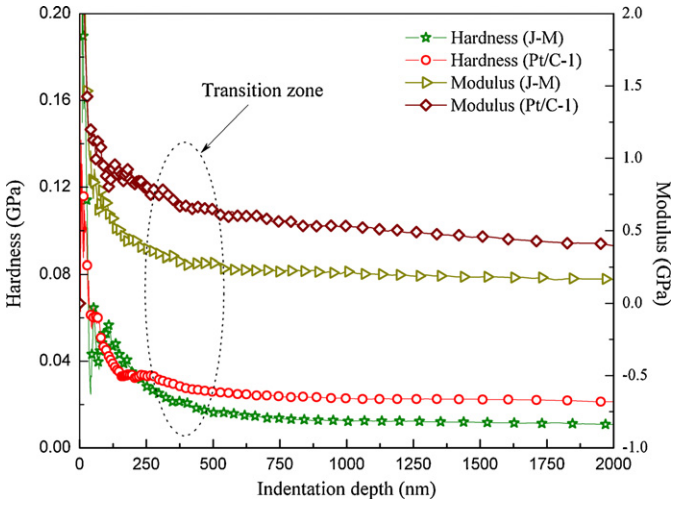

Fig. 5. Modulus and hardness response of two CLs as a function of depth.

results show negligible changes in physical properties, they cannot be used to assert the difference in the mechanical properties, if any, of J–M and Pt/C-1.

5.2. Mechanical characterization

Mechanical properties such as modulus and hardness are obtained directly from the experiments. Relations mentioned in Section 3 are used to estimate reduced modulus and contact stiffness. For a graded material, these properties change with the indentation depth.

Fig. 4 shows the indentation curves for Pt/C-1 as well as J–M catalyst layers and this provides information in terms of displacement and load. Each curve can be divided into three segments – loading, holding (dwell), and unloading. There is a 10 s dwell period introduced to evaluate the possibility of creep characteristics in CL. Interestingly, both CLs show a displacement at constant load. It is worth noting that nafion is a visco-elastic material that shows creep characteristics even at room temperature [24,25]. Hence, nafion constituent present in the CL gives rise to creep behavior in CLs. This is however, an entirely different direction of research which this study not focusing on. Indentation array was performed at different vicinity of CL at different depth levels (1800–2000 nm). However, averaged curve for each samples (J–M and Pt/C-1) are shown in Fig. 4. In both the CLs, loading and displacement relation is nonlinear (large displacement at low load, which may have happened from the plastic deformation). Hence, it can be concluded that the current CLs under investigations are unlikely to show brittle characteristics. This can be further confirmed from the dwell period in Fig. 4. Displacement under constant load in ductile materials is more obvious phenomenon than in brittle materials. Loading curve is used to calculate the averaged modulus and hardness of the layer. Unloading curve is used to get averaged reduced modulus (Section 3). The physical importance of reduced modulus is that it is a quantification of elastic deformation occurring in both CL and the indenter. Averaged values of hardness, elastic modulus, and contact stiffness are listed for each experimental trial in Table 1. Elastic–plastic loading followed by elastic unloading is observed in both the cases. However, difference can be made in terms of maximum indentation load. Low indentation load on commercial CL appears to make a large indentation depth as opposed to Pt/C-1. The possible explanation for this can be derived after analyzing Fig. 5.

Fig. 5 explains about the variation in hardness and modulus over the indentation depth of 2000 nm. Though initially for J–M catalyst, hardness values are slightly higher than the Pt/C-1, its value reduces to around 0.02 GPa beyond 350 nm. High initial values are attributed to the indenter encountering the densely packed carbon supported catalyst particles on a surface level. At a much lower depth (>350 nm), indenter interacts with less number of particles. Hence, softness induced by the binder (nafion) material would lead to large displacement at a low load (J–M, Fig. 4) resulting in a reduced amount of hardness in CL as a function of depth. There is a smooth variation in the mechanical properties of both CLs beyond the transition zone.

From Figs. 4 and 5, two major observations can be highlighted. Firstly, difference in the values of obtained mechanical properties and secondly, gradation in obtained mechanical properties.

Table 1
Experimentally obtained mechanical properties (averaged) of CLs.

Catalyst	Trials	E_s (GPa) (average modulus)	Mean E_s (GPa)	H (GPa) (average hardness)	Mean H (GPa)	S (N m^{-1}) (average stiffness)	E_r (GPa) (reduced modulus)
J–M	1	0.451	0.492	0.0257	0.0326	643.755	0.466
	2	0.481		0.031		623.5329	0.497
	3	0.523		0.039		641.0351	1.12
	4	0.514		0.035		740.2246	1.035
Pt/C-1	1	0.787	0.737	0.052	0.0436	1612.187	1.68
	2	0.756		0.048		1523.834	1.52
	3	0.709		0.0375		1322.309	1.42
	4	0.697		0.037		1455.183	1.40

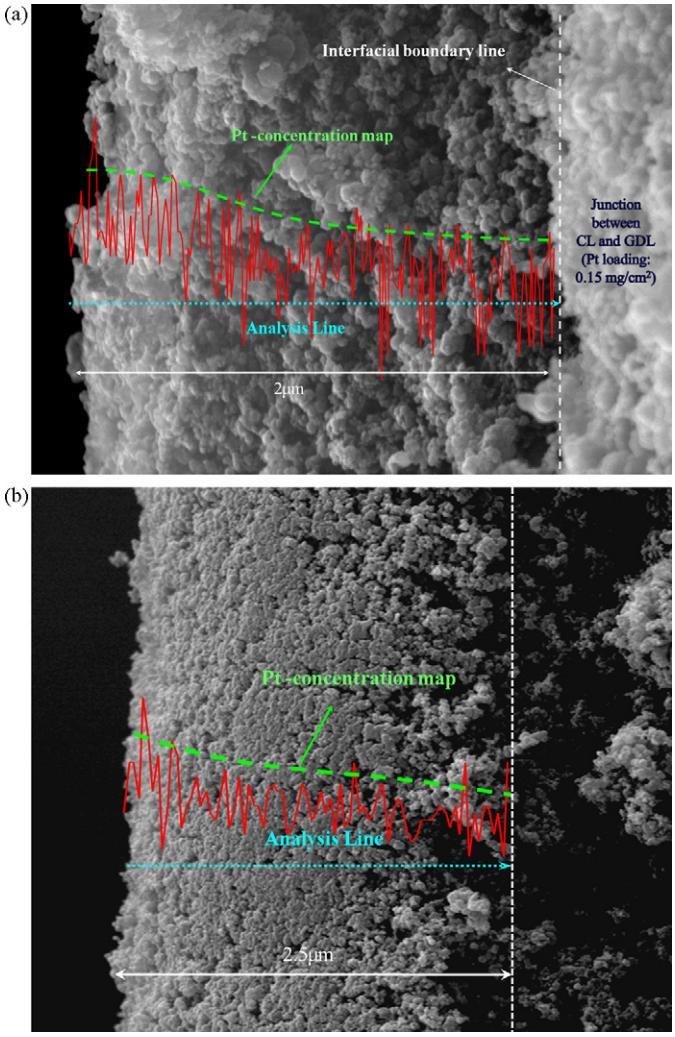

Fig. 6. SEM cross-section image and EDAX line analysis to determine the Pt concentration throughout the layer thickness for (a) J–M catalyst. (b) Pt/C-1.

Observed difference between J–M and Pt/C-1 values in terms of obtained mechanical properties is attributed to the type of carbon support (Vulcan and J–M) that is used to fabricate CL. While, observed gradation in mechanical properties of both CLs are attributed to the Pt or carbon particle distribution throughout the layer.

Fig. 6(a) and (b) shows the SEM cross-section of CL and this provides a supporting explanation for change in the mechanical properties. EDAX line analyses are conducted to obtain the Pt concentration throughout the CL thickness (about 2 μm) (Fig. 6(a) and (b)). It can be observed that the Pt concentration changes from outer to the inner surface gradually and is analogous to the obtained mechanical property variations (Fig. 5). Hence, it is perceived from our study that the nano-level composition distribution in CL affects the mechanical property variations.

Further, as previously mentioned, indentation of catalyst surface by a sharp indenter provides quantitative information related to contact stiffness that can be referred to an amount of resistance that the material can withstand from an external force in the normal direction. Fig. 7 shows the contact stiffness data as a function of indentation depth for both the CLs (J–M and Pt/C-1). Three contact stiffness curves for each CL are provided. Significant increase in the contact stiffness is observed in case of Pt/C-1. Near – linear relationship in the contact stiffness with the indenter displacement can be observed in Pt/C-1 up to some initial depth, however, in J–M,

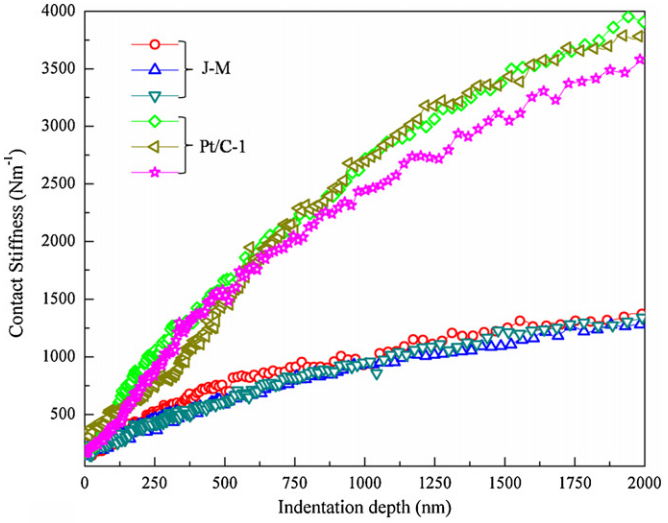

Fig. 7. Contact stiffness variations as a function of depth in two catalysts. Decrease in slope can be observed in J–M catalyst after 300 nm. In case of Pt/C-1 slope increases after 250 nm and again falls beyond 850 nm.

contact stiffness starts to follow a nonlinear relationship with the indenter displacement from the top surface itself. Beyond some initial depth, in case of Pt/C-1, slope of stiffness curve decreases slowly with a value much higher than the J–M.

Current indentation technique cannot be used to estimate the number of particles or particle size; however, it gives an understanding of particle distribution. Although both of the CL's have a Pt loading of 20 wt%, its distribution throughout the depth becomes influential on change in properties. Causes for variation in mechanical properties can be summarized as follows. Berkovich indenter having a tip radius of about 100 nm (confirmed from AFM scan) encounters with the Pt supported carbon particles (≈30 nm). Within its tip radius boundary, it may encounter pores, aggregated Pt particles on carbon support or uniform/non-uniform distribution of carbon particles itself. Hence, values of hardness, modulus, and contact stiffness obtained in terms of indentation depth are influenced by the indenter's interaction with the layer constituents, and their nature of distribution. In case of J–M, slope of stiffness is observed to be decreasing over a depth and, for Pt/C-1, it decreases gradually with much higher contact stiffness as compared to J–M. This is a valid observation and it indicates a perfect gradation in J–M catalyst whereas in Pt/C-1 it is near homogeneous. Details presented here can be further consolidated from Fig. 6(a) and (b).

5.3. Numerical analyses

Since, J–M as well as Pt/C-1 show a decreasing gradation from the outer surface (equivalent to membrane side) to the inner surface (GDL side), only the mechanical properties of Pt/C-1 are taken for numerical analyses (in Section 5.3, CL refers to Pt/C-1). A nonlinear FE model is analyzed for single CL as well as dual-layer comprised of membrane and CL. Since the indentation of CL involves elastic–plastic loading with a residual impression upon unloading, considerable interest is shown in finding the yield strength of CL that may provide valuable information related to plastic deformation. The best possible way to fulfill this requirement is through FE Analyses. As mentioned earlier, the yield strength of CL is obtained from the simulation results. Several trials were run to fit the experimental load–displacement values, exactly. Red-dotted line in Fig. 4 represents the load–displacement curve for Pt/C-1 obtained from numerical simulation. Corresponding yield strength value taken in elastic–perfectly plastic numerical model

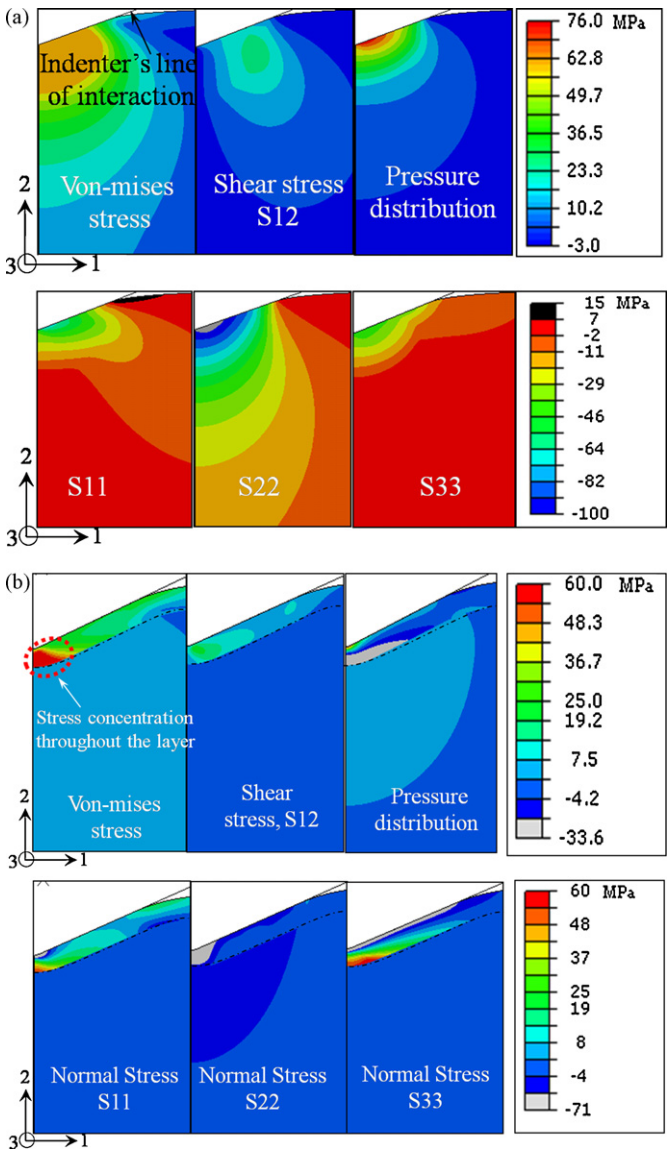

Fig. 8. (a) FE results of stress contours and pressure distributions in a discrete CL model under loaded condition. Von-mises stress, radial stress distribution (S11), normal stress plane perpendicular to 2-axis (S22), circumferential stress (S33), shear stress (S12), and hydrostatic pressure field distributions can be observed in CL. (shaded grey region in S22 refers to less than the minimum value in the color bar). (b) Stress contours and pressure distribution in dual-layer discrete model. It is noted here that S33 > S11, condition for promoting radial cracking.

to achieve a consistency between the experimental and simulation results was found to be around 50–60 MPa. Average elastic modulus was taken to be 0.5 GPa (see Table 1) with a Poisson's effect of 0.18. It becomes easier now to predict the yield strength values for a graded model. Hardness values obtained as a depth function (shown in Fig. 5) are scaled down to obtain the corresponding yield strength values for the CL. Constant displacement approach is applied to all analyses. Indenter is made to displace 5 μm from the catalyst surface and corresponding reaction force response is recorded.

5.3.1. FEA under non-graded condition

In this first part of analyses, single CL is chosen and is assumed to have near-infinite thickness. Average mechanical properties listed in Table 1 are taken along with the yield strength value of 60 MPa. Fig. 8(a) shows the stress contours for a CL upon indentation. Force required by the indenter for 5 μm penetration was approximated to be 0.35 mN (not shown in figure for the brevity). To characterize the effect of multiple layers on the stress distribution/transfer, indentation of CL along with nafion membrane is preferred. Here, thickness of CL and membrane is taken to be 2 and 50 μm, respectively. Fig. 8(b) shows the stress contours in discrete dual-layer system. Interestingly, force required to penetrate the same distance of 5 μm is observed to be far less than the case of single CL. It was around 3.5 μN. A possible explanation for this can be as follows: yield strength of nafion membrane is very less compared to CL. Because of this, plastic deformation induced in the membrane is larger and this tries to accommodate the induced indentation force.

Failure studies of the layers require detailed information regarding normal stress distribution directions. Hence, contour plots of directional stresses (S11 (radial stress, also referred as normal stress plane perpendicular to 1-axis), S22 (normal stress plane perpendicular to 2-axis), and S33 (circumferential stress, also referred as normal stress plane perpendicular to 3-axis)) along with the shear stresses (S12) are given in Fig. 8(a) and (b). Directional stresses are plotted as to differentiate the response of monolayer model from the dual-layer model, subjected to indentation. Further, micro-indentation study conducted by Lee et al. [26] reveals the circumferential cracks in CL. Prediction of crack initiation in a layer requires the knowledge of radial stress (S11) and circumferential stress (S33) distributions. A maximum value of radial stress, S11, found here in single CL (Fig. 8(a)) is comparatively larger than S33. Although this condition promotes circumferential cracking, it is perceived to be advantageous as it locally restricts the deformation to the indented region. However, dual-layer model's response gives distinguished results altogether. It is noted from Fig. 8(b), that S11 is less than S33 – a condition that can promote a radial cracking in CL. Further, this can be lethal in initiating the interfacial cracks in bonded region between membrane and CL. Decrease of S11 and increase of S33 from monolayer model to the dual-layer model is caused due to the presence of membrane layer in the dual-layer model. Hence, plotting of directional stresses reveal changes in stress levels that might have influenced by the material response of the adjacent bonded layer (here membrane). Moreover, it is important to know the normal stress, S22, and shear stress, S12, variations upon unloading. This has to explain with the interfacial behavior of dual-layer systems. It is observed from our numerical study that, unloading leads to an increased value of interfacial normal stress (S22) as shown in Fig. 9. Though shear stress value was found to be decreasing after unloading, its magnitude was still large enough to initiate an interfacial damage. Plastic strain (PEEQ, measure of plastic deformation) after unloading is also shown in Fig. 10. Contours of discrete dual-layer system indicate a large plastic deformation in nafion membrane. (It is noted that the normal stress, S22, distribution would show a high negative value (greater than the radial stress, S11) as the indenter's interaction with the surface is in the direction exactly opposite to that of axis-2. Further, one may observe the contours of hydrostatic pressure distribution are just opposite to that of normal stresses, especially S22. This is because, S22 and pressure act in the opposite directions to each other.)

5.3.2. FEA under graded condition

In the following, gradation (increasing gradation from the top surface to the bottom surface as viewed from the membrane) in CL is considered and FEA procedure followed here is similar to previous section except the mechanical property variations. Fig. 11 shows the contour plot of graded dual-layer system considering the gradation. It can well be distinguished from the discrete model in terms of stress concentration distribution in CL. Stress contours are not concentrated to specific area as opposed to discrete model. Here also S33 was found to be greater than S11 like in the case of dual-layer discrete model, however, it was distributed near the

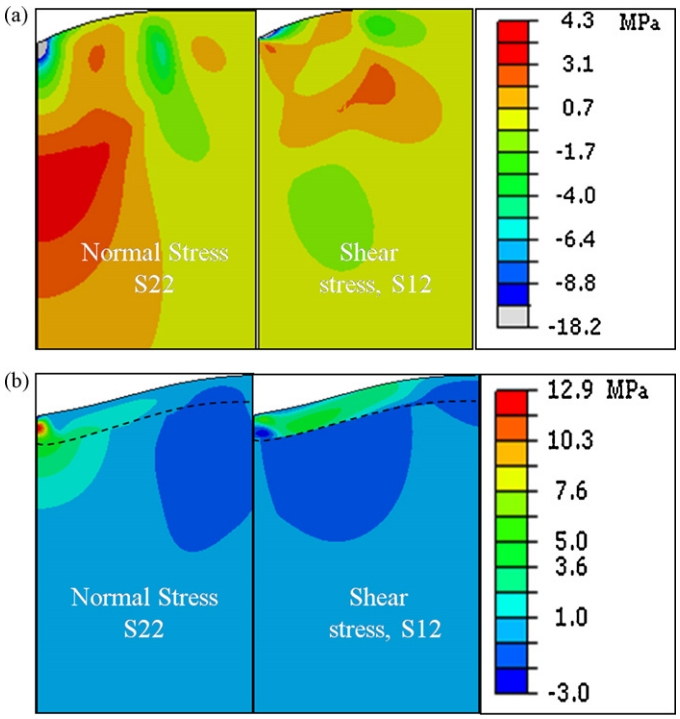

Fig. 9. Effect of unloading on the normal stress (S22) and shear stress (S12) distribution in (a) discrete CL model (b) non-graded dual-layer model.

interface line (normal stress contours in this case are not shown for the brevity, also von-misses stress distribution is sufficient to explain the stress redistribution phenomenon). Due to low modulus near the surface level, local stress concentration resulting from damage nucleation (a direct effect of plastic deformation) and continuously increasing mechanical properties spread the stress values interior to the layer. Because of this, we see stress redistribution near the interfacial line. Further, continuously increasing mechanical properties (modulus and yield strength) of a material from the surface to the bottom make this CL a good damage resistant and thus can sustain a greater amount of load as compared to homogeneous counterpart. Overall plastic equivalent strain after unloading in graded dual-layer model and discrete dual-layer model remains to be almost same (maximum of 71% and 66%, respectively) as shown in Fig. 10. This is however, an indication that graded material can withstand very high stress values as compared to its homogeneous counterpart by causing an almost same plastic strain in the adjacent layer (here membrane). On the other hand, sudden jump in stress values seen between CL and membrane separated by an interfacial line could initiate an interfacial fracture and thereby causing a total failure over many loading cycles. Though stress values are found to be higher, stress redistribution near the interface certainly increases the toughness and damage resistance of the layer; however, this may not guarantee the fact that the interfacial zone is not vulnerable to delaminations or crack propagations.

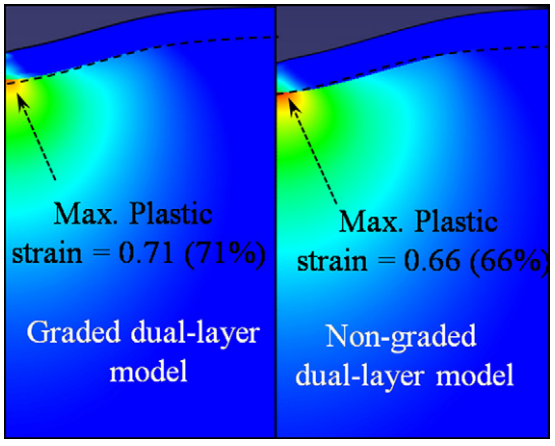

Fig. 10. Plastic strain (PEEQ) distribution in both the graded as well as non-graded dual-layer model. Maximum plastic strain is observed to be almost same for both the models.

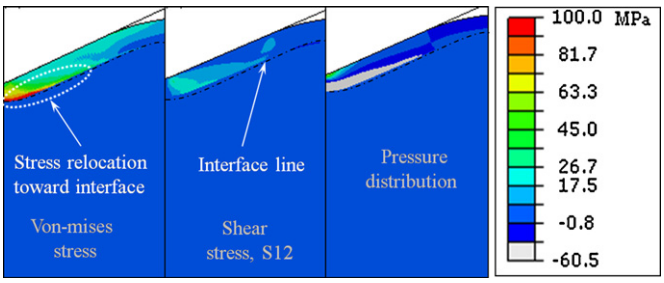

Fig. 11. Stress and pressure distribution in the graded dual-layer model subjected to indentation loading cycle. Stress redistribution near the interfacial line can be observed here.

In the above gradation model, surface side of CL is assumed to have a low modulus and hardness as compared to its bottom. The condition may be reversed to follow a smooth force transition between CL and membrane; however, at this stage we neglect it (this effect may draw distinguished results and conclusions). Spray coated CL on GDL is used for the indentation experiment and CL's surface side is found to give high modulus and hardness as evident from Fig. 5. In addition, it is believed that this surface of the CL encounters with the membrane when the layers are stacked together. Hence, in our numerical model, contacting interface of CL is given high values of mechanical properties to imitate a real situation. Consideration of GDL as a separate layer is avoided in the present model while complete focus is given to CL.

Plastic energy dissipation (in Joules) of all developed models is represented in Fig. 12(a) for loading as well as unloading cycles. Discrete monolayer model is observed to dissipate large amount of plastic energy (which is also a measure of damage factor) as compared to dual-layer graded models (however, its role is very insignificant in estimating the damage related failures unless we know the contributions of each layer). Interestingly, both dual-layer models (graded and discrete) are found to dissipate almost same amount of plastic energy. However, a slight increase in energy dissipation can be seen after unloading in graded dual-layer model, but it is too small to be considered in drawing any conclusion. Concentrating further on CL itself in dual-layer models, greater amount of energy dissipation was observed to be evident in case of plastically graded dual-layer model as shown in Fig. 12(b). This specifically suggests that the geometrical heterogeneity may have played a very significant and advantageous role in enhancing the ductility of CL. Now, for developed models, energy balance equation mentioned in Eq. (8) can be met and it is evident from the Fig. 12(b) (IE = EE + PDE). Further, elastic contribution is found to be larger than plastic energy dissipation. From Eq. (10), ratio of elastic to plastic contribution is likely to be larger than one. Hence, deformation is dominated by the elastic part.

In summary, stress relocation toward an interface may toughen CL from being penetrated, however this may also increase the chances of damage evolution and interfacial damage between the layers. Further, local mechanical strain caused due to heterogeneity in CL may affect the mass transfer characteristics as well. The results presented in this article on the mechanical properties of CL can be extended to approach a driving force for crack or interfa-

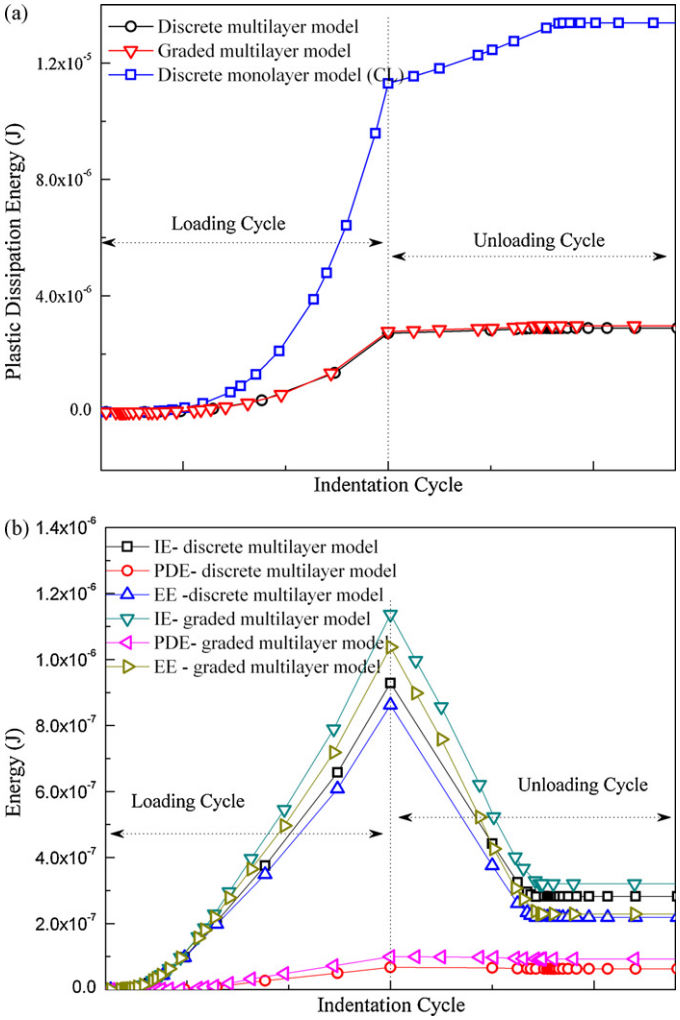

Fig. 12. (a) Plot of plastic energy dissipation over one complete indentation cycle for all developed models. (b) Energy plots of CLs involved in two models (graded and discrete) over one complete indentation cycle. Plot shows variations in internal energy (IE), plastic dissipation energy (PDE), elastic energy (EE) for two models. Energy balance mentioned in Eq. (8) is achievable throughout the cycle.

cial adhesion strength/shear strength or interfacial stress intensity factors using the linear fracture mechanics principles.

6. Concluding remarks

Nanoindentation is successfully used in extracting the contact stiffness, hardness, and modulus of the CLs as a depth function. Gradation in CL was unintentional, and it was only after experimental investigation found to belong to graded class of materials. Experimental investigation coupled with numerical simulation gives valid information regarding stress concentration and plastic deformation in CL and membrane. Comprehensive structural analyses of CL have been conducted in addition to its effect on bonded layer (membrane). Yield strength of CL is estimated from experimental combined numerical approach (60–70 MPa). On a most important note, CLs studied here are found to exhibit ductile characteristics and hence these are prone to ductile damage upon plastic deformation accumulation over many loading cycles (mechanical or hygrothermal or freeze/thaw cycle). This is however, a contradicting observation to the conventional belief that the CLs are brittle materials [27]. Although there are models to predict the failure of fuel cell layers, fundamental understanding of the evolution of cracks and delaminations lies in the nature of the layer properties and its limitations on force transferring characteristics.

Further, force required to penetrate a distance of 5 μm in dual-layer model is estimated to be hundred times less than the single layer CL model. Significant variations among the three developed models are seen in terms of stress concentrations and plastic deformations. Plastic strain was observed to be similar in both the graded and discrete models. This suggests that the graded model (with an increasing gradation toward membrane) could withstand higher amount of stresses. In addition, increased plastic energy dissipation suggests increased ductility. However, this may not guarantee the fact that the interfacial layer is damage proof. Stress relocation toward the interface can be an indication for the root cause of interfacial failure. This prompts us to study further on the damage evolution in fuel cell layers and it is reported in part 2.

Not all CLs belong to a graded class of materials. However, procedure adopted here can be used to quantify the mechanical stresses and plastic deformations in catalyst layers that may further proceed to cause damage evolution near the interfaces. Between J–M and Pt/C-1, J–M is found have more graded than Pt/C-1. Hence, Pt/C-1 can be referred as a near-homogeneous material.

Acknowledgements

This work was supported by Inha University. Authors are thankful to 'Inha Collaborative Research Instruments' for providing necessary information in using the experimental devices.

References

[1] S. Suresh, Science 292 (2001) 2447–2451.
[2] K.D. Jandt, Nature Materials 7 (2008) 692–693.
[3] K. Tai, M. Dao, S. Suresh, A. Palazoglu, C. Ortiz, Nature Materials 6 (2007) 254–262.
[4] K.S. Kumar, H. Van Swygenhoven, S. Suresh, Acta Materialia 51 (2003) 5743–5774.
[5] I.S. Choi, Indentation of plastically graded materials, PhD Thesis, MIT, 2007.
[6] S. Kundu, M.W. Fowler, L.C. Simona, S. Grot, Journal of Power Sources 157 (2006) 650–656.
[7] F.A. de Bruijn, V.A.T. Dam, G.J.M. Janssen, Fuel Cells 08 1 (2008) 3–22.
[8] D. Bograchev, M. Gueguen, J.C. Grandidier, S. Martemianov, International Journal of Hydrogen Energy 33 (2008) 5703–5717.
[9] Y. Tang, M.H. Santare, A.M. Karlsson, S. Cleghorn, W.B. Johnson, Journal of Fuel Cell Science and Technology 3 (2) (2006) 119–124.
[10] A. Kusoglu, A.M. Karlsson, M.H. Santare, S. Cleghorn, W.B. Johnson, Journal of Power Sources 161 (2) (2006) 987–996.
[11] A. Kusoglu, A.M. Karlsson, M.H. Santare, S. Cleghorn, W.B. Johnson, Journal of Power Sources 170 (2) (2007) 345–358.
[12] Q. Wang, M. Eikerling, D. Song, Z. Liu, T. Navessin, Z. Xie, S. Holdcroft, Journal of Electrochemical Society 151 (7) (2004) 950–957.
[13] Z. Xie, T. Navessin, K. Shi, R. Chow, Q. Wang, D. Song, B. Andreaus, M. Eikerling, Journal of Electrochemical Society 152 (6) (2005) 1171–1179.
[14] G. Feng, W.D. Nix, Y. Yoon, C.J. Lee, Journal of Applied Physics 99 (2006) 074304.
[15] X. Li, H. Gao, C.J. Murphy, K.K. Caswell, Nano Letters 3 (2003) 1495–1498.
[16] E.P.S. Tan, C.T. Lim, Applied Physics Letters 87 (2005) 123106.
[17] S. Logothetidis, S. Kassavetis, C. Charitidis, Y. Panayiotatos, A. Laskarakis, Carbon 42 (2004) 1133–1136.
[18] M. Lucas, W. Mai, R. Yang, Z.L. Wang, E. Riedo, Nano Letters 7 (2007) 1314–1317.
[19] M.L. Oyen, Journal of Biomechanics 39 (2006) 2699–2702.
[20] D.M. Ebenstien, L.A. Pruitt, Nanotoday 1 (2006) 26–33.
[21] X. Li, B. Bhushan, Scripta Materialia 42 (2000) 929–935.
[22] A.C. Fischer-Cripps, Nanoindentation, Springer, New York, USA, 2002.
[23] ABAQUS, Analysis User's Manual, Hibbitt, Karlsson & Sorensen, Inc., 2007.
[24] M.B. Satterfield, P.W. Majsztrik, H. Ota, J.B. Benjiger, A.B. Bocarsly, Journal of Polymer Science: Part B: Polymer Physics 44 (2006) 2327–2345.
[25] P.W. Majsztrik, A.B. Bocarsly, J.B. Benjiger, Macromolecules 41 (2008) 9849–9862.
[26] G. Lee, H. Lee, D. Kwon, Electrochimica Acta 52 (12) (2006) 4215–4221.
[27] Y. Li, J.K. Quincy, S.W. Case, M.W. Ellis, D.A. Dillard, Y.H. Lai, M.K. Budinski, C.S. Gittleman, Journal of Power Sources 185 (2008) 374–380.